JACS
JOURNAL OF THE AMERICAN CHEMICAL SOCIETY
Article
pubs.acs.org/JACS

Core/Shell Colloidal Semiconductor Nanoplatelets

Benoit Mahler,[†] Brice Nadal,[†] Cecile Bouet,[†] Gilles Patriarche,[‡] and Benoit Dubertret*,[†]

[†]Laboratoire de Physique et d'Etude des Matériaux, CNRS, ESPCI, 10 rue Vauquelin, 75005 Paris, France
[‡]Laboratoire Photonique et Nanostructures, CNRS, 91460, Marcoussis, France

Supporting Information

ABSTRACT: We have recently synthesized atomically flat semiconductor colloidal nanoplatelets with quasi 2D geometry. Here, we show that core/shell nanoplatelets can be obtained with a 2D geometry that is conserved. The epitaxial growth of the shell semiconductor is performed at room temperature. We report the detailed synthesis of CdSe/CdS and CdSe/CdZnS structures with different shell thicknesses. The shell growth is characterized both spectroscopically and structurally. In particular, the core/shell structure appears very clearly on high-resolution, high-angle annular dark-field transmission electron microscope images, thanks to the difference of atomic density between the core and the shell. When the nanoplatelets stand on their edge, we can precisely count the number of atomic planes forming the core and the shell. This provides a direct measurement, with atomic precision, of the core nanoplatelets thickness. The constraints exerted by the shell growth on the core is analyzed using global phase analysis. The core/shell nanoplatelets we obtained have narrow emission spectra with full-width at half-maximum close to 20 nm, and quantum yield that can reach 60%.

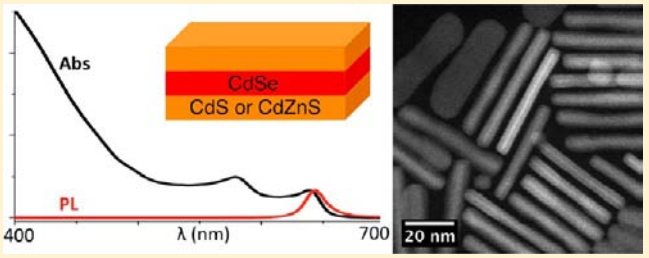

INTRODUCTION

Semiconductor nanocrystals (NCs) exhibit unique physical properties that depend chiefly on their size.[1] For colloidal NCs, the size-dependent optical properties were first reported for nanoparticles with spherical shapes and a three-dimensional (3D) confinement,[2] but were later extended to nanorods[3] or nanowires[4] (2D confinement) and recently to nanoplatelets (NPLs, 1D confinement).[5] The optical properties of core-only structures are greatly improved when a semiconductor shell is epitaxially grown on the core. In particular, the growth of a shell on core NCs can enhance their quantum yield[6] and the resistance to photobleaching,[7] and reduce fluorescence emission blinking at the single particle level.[8,9] Such properties have led to a growing use of core/shell nanocrystals as luminescent biological probes[10] and as active materials in light emitting diodes,[11] or in optoelectronic devices.[12]

In spite of the advantages of core/shell structures, their synthesis is complex and several difficulties need to be addressed. First, the lattice mismatch between the core and the shell induces pressure on the core that can reach up to 4 GPa in spherical CdS/ZnS core/shell NCs.[13] This pressure buildup with lattice mismatch has been recently used to tune the optical properties of some core/shell structures,[14] but generally, the epitaxial growth of two materials with large lattice mismatch induces crystal defects and prevents thick shell growth.[15] Second, the core/shell interface is hard to control precisely, because cations[16] and anions[17] may diffuse during the shell growth. The control of the interface is important, because it was recently realized that a composition gradient between the core and the shell[18] further suppresses the Auger processes, reduces blinking,[19] and improves the fluorescence quantum yield. Third, the type of ligands used for the shell growth can influence the shape of the final nanostructure,[20,21] as well as the crystal structure of the shell that can be different than that of the core.[22,23] In addition, the 2D NPLs need to be handled with great care to avoid their degradation[24] and/or their transformation into spheres or rods during the shell growth.

In spite of these difficulties, epitaxial core/shell structures have been grown on cores of different compositions[25,26] and shapes, including spheres and nanorods.[27] In the case of spherical cores, a fine-tuning of the ligands used during shell growth gives access to core/shell nanocrystals that can have a spherical shape, a rod shape[21] (dot in rod core/shell structures), or a disk shape[28] (dot in plate core/shell structures). So far, the growth of a shell on a quasi 2D system such as nanosheets or nanoplatelets has not been realized. The growth of an epitaxial shell on a nanoplatelet is highly desirable, since it would introduce the possibility of colloidal synthesis of multiple quantum wells[29] and would provide a useful method to improve the quantum yield and the robustness of the nanoplatelets emission.

In this paper, we report the synthesis of core/shell nanoplatelets using a novel shell growth method at room temperature. We first report the possibility of exchanging the ligands on the NPLs while preserving their 2D structure. We then extend this approach to develop a layer-by-layer deposition method for the growth of a monolayer CdS shell. Finally, we modify this method to make continuous growth of a CdS and a CdZnS shell that can be up to 2 nm thick on CdSe

Received: August 9, 2012
Published: October 12, 2012

   dx.doi.org/10.1021/ja307944d | J. Am. Chem. Soc. 2012, 134, 18591−18598

NPLs. These core/shell structures are characterized using high-resolution TEM, as well as photoluminescence (PL).

RESULTS AND DISCUSSION

To develop the ligand exchange protocols, as well as the core shell syntheses, we have mainly used 512 nm emitting CdSe nanoplatelets. We synthesized them using the same protocol as the one described in 2008.[5] We obtain NPLs with lateral dimensions ~10 nm × 35 nm and a thickness that is controlled with atomic precision. These NPLs have a zinc blende structure, and their two largest facets end with a cadmium-rich plane passivated by carboxylate ligands.[5,24] They are structurally significantly different from the nanoribbons[30] or the quantum belts[31] that have wurtzite structure and largest facets formed with a stoichiometric mixture of anions and cations.[24] The zinc blende NPL thickness is in the ⟨100⟩ direction, and the lateral sides are perpendicular to the ⟨010⟩ and the ⟨001⟩, direction respectively.[32]

Ligand Exchange on CdSe NPLs. The first step that we explored in our route to synthesize core/shell NPLs is the possibility of exchanging the NPL ligands while maintaining the 2D geometry. The carboxylate ligands, that are bound on the Cd-rich facets, can, in principle, be replaced, as is the case with spherical NCs, with other Cd binding ligands through proton exchange.[33] We tested ligand exchange on the NPLs using dodecanethiol (Figure 1a). After 24 h, in an excess of dodecanthiol, the NPL solution changed color. The NPL absorption spectrum retains similar features as those before ligand exchange, but is overall shifted about 30 nm to the red (Figure 1b). To the best of our knowledge, such a large red shift (130 meV) of the first excitonic transition after ligand exchange has not been reported so far. This strong shift can be explained if we consider that the 1D confinement of the exciton, originally limited to the CdSe, extends into the two additional monolayers of the thiolate functions once the ligand exchange is complete. Indeed, the first exciton absorption wavelength (542 nm) after the addition of two sulfur layers on the NPLs is close to the first exciton absorption wavelength (553 nm[34]) when one CdSe monolayer is added. In spherical or rod-shaped nanoparticles, the outer facets are composed of several crystalline orientations, and a thiol ligand exchange is not effective on all facets, which reduces the overall size increase and hence the red shift.[35] After ligand exchange, the NPLs are still fluorescent, but their quantum yield has dropped by half to 15%. Such a quantum yield is unexpected and contrasts with previous studies on isotropic CdSe nanocrystals coated with alkylmercaptans that have little if any fluorescence.[36] The full-width at half-maximum (fwhm) of the NPL emission spectrum is still very narrow (<10 nm), and suggests that the NPLs have not degraded into nanocrystals with another geometry such as sphere or rod that have much larger fwhm. The conservation of the NPL shape after the dodecanethiol treatment is confirmed with the TEM images (Figure 1d), where the NPLs appear mostly aggregated and twisted. We have analyzed the thiol ligand exchange with IR spectroscopy (Figure 1e). The two peaks at 1500 cm^{-1} and 1400 cm^{-1}, characteristics of the carboxylate function, disappear, while a sharp peak at 1450 cm^{-1}, characteristic of the thiol function, appears. We conclude that ligand exchange is possible on NPL while maintaining its 2D geometry and most of its optical properties.

Layer by Layer Growth of a CdS Monolayer on CdSe NPLs. The ligand exchange with the dodecanthiol is a method

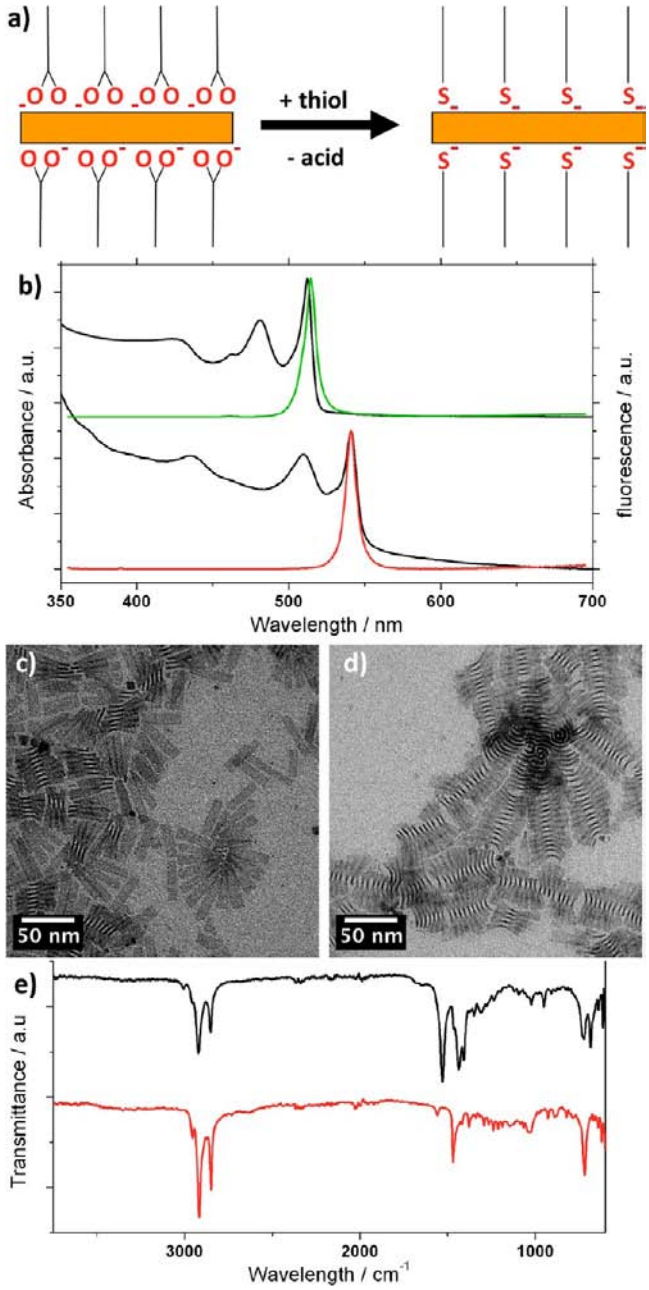

Figure 1. (a) Schematic representation of the ligand exchange with dodecanethiol. (b) Absorbance (black) and fluorescence (colored) of the nanoplatelets solution before (top) and after (bottom) ligand exchange. TEM pictures of the NPLs (c) before and (d) after the ligand exchange. (e) FTIR spectra of the NPLs before (black) and after (red) ligand exchange with dodecanethiol.

to coat the NPL facets with thiolates. This ligand exchange provides a nice method to add a sulfide layer on each main facet of the NPLs, but the thiolate blocks further growth, at least at room temperature. In order to coat the NPLs with an anion layer that could serve as a substrate for additional reactions, we have used a bis-trimethylsilylated (TMS_2S) sulfur precursor[37,38] that has the ability both to react selectively with the carboxylate ligands at the surface of the NPLs to displace it and to replace the oxyanionic ligand with a TMS-S bound on a cadmium atom at the surface. When the TMS_2S is introduced in the NPL solution, the NPLs aggregate rapidly and the solution changes color from yellow to orange. The absorption spectrum of the

dx.doi.org/10.1021/ja307944d | J. Am. Chem. Soc. 2012, 134, 18591−18598

aggregated NPLs is reported Figure 2b (middle). As for the exchange with dodecanthiol, we observe a red shift on the

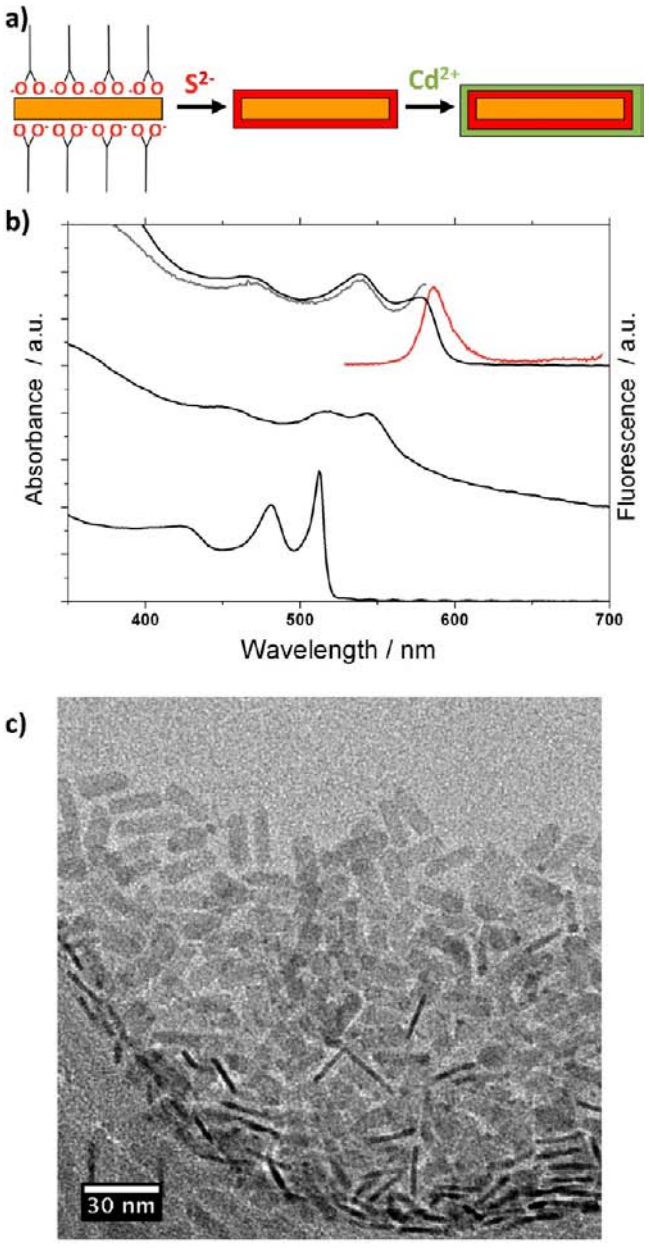

Figure 2. (a) Schematic representation of the layer-by-layer CdS shell growth on a CdSe NPL. (b) In black, absorbance spectra of the original CdSe NPLs (bottom), after reaction with TMS_2S (middle) and after reaction with TMS_2S, and then with cadmium acetate (top). (red) Fluorescence and (gray) photoluminescence excitation spectra of CdSe/CdS NPLs (top). (c) TEM picture of the final CdSe/CdS core/shell NPLs.

absorption spectrum of the NPL solution after reaction with the TMS_2S. However, the heavy-hole and light-hole transition peaks, corresponding to the first two electronic transitions,[5] are not as sharp as in the case of core-only NPLs or after coating with dodecanethiol. This broadening of the excitonic transitions may be due to thickness and/or ligand density variations between NPLs. It may also be related to the aggregation of the NPLs. After this first step, the NPL solution is washed twice by precipitation with ethanol to remove the excess of TMS_2S. This washing step also breaks the remaining TMS-S bonds and produces reactive, sulfide-rich surfaces. We then introduce successively in the reaction vessel a solution of cadmium acetate and an excess of oleic acid to complete the second step of the CdS monolayer growth. The cadmium ions react with the facets of the NPLs (Figure 2a) and induce another red shift of the NPL absorption spectrum to 578 nm (Figure 2b, top), consistent with the growth of a CdS layer. These CdSe/CdS NPLs are fluorescent with an emission maximum at 586 nm. During the CdS deposition, the Stokes shift between the first excitonic transition and the emission maximum increases from ~1 nm to ~8 nm, and the fwhm increasese from ~8 nm to ~20 nm. These changes could be due to uneven CdS coating of the NPL surface. The integrity of the NPL shape after shell growth is visible in Figure 2c, where NPLs appear either flat on the TEM grid or standing on their edge. These CdSe NPLs coated with one CdS layer demonstrate the possibility to synthetise core/shell NPLs. The synthetic scheme developed here is very general and can be applied to other types of precursors and shell materials as long as the surface and the precursor reactivity are high. For example, we have successfully overcoated CdSe nanoplatelets with a monolayer of zinc sulfide by replacing cadmium acetate by zinc acetate in the shell deposition protocol (see Supporting Information for detailed protocol, Figures S1 and S2 for spectroscopic characterization and TEM picture, respectively). Moreover, the TMS_2S can also be replaced by other sulfide precursors such as hydrogen sulfide H_2S (Figures S5 and S6 in Supporting Information) or ammonium sulfide $(NH_4)_2S$ (Figures S3 and S4 in Supporting Information). In these last two cases, the protocols are slightly modified and can take place in biphasic mixtures (see Supporting Information for details). These experiments demonstrate the feasibility and versatility of the low-temperature shell growth on nanoplatelets using a layer-by-layer approach.

CdSe/CdS NPLs with Continuous Shell Growth. The possibility of growing with a layer-by-layer process a first CdS or ZnS layer on a CdSe NPL prompted us to develop a method for the continuous growth of shell in a "one pot"-type approach. Layer by layer processes are very useful when a fine control of the shell composition is needed in the case, for example, of formation of a gradient[39] or multishell structures,[40] but when thick shells are needed, the application of a layer-by-layer protocol can be time-consuming.[8] In particular, in the protocols exposed above, the nanocrystals need to be carefully washed between each layer to avoid secondary nucleation. In order to realize a "one-pot" growth of thick shells, we developed a protocol in which all the precursors necessary for shell growth are directly introduced in the NPL solution. For this process, we have used a mixture of thioacetamide (TAA) and octylamine as a source of sulfur and cadmium oleate as a source of cadmium. A mixture of TAA and octylamine is first added in the NPL solution to initiate the deposition of a sulfur layer. Indeed, the octylamine is expected to react with thioacetamide to form *N*-octyl-ethanimidamide and to release H_2S[41] which can then react with the cadmium at the surface of the NPLs. An excess of octylamine with respect to TAA is used so that both the formation of ammonium sulfide complex in solution and the stabilization of the NPLs once they have reacted with the sulfide are ensured. After this first step that lasts for 10 min, the source of cadmium is added. Since the TAA has good solubility in the chloroform/octylamine mixture, the system we use for the shell growth,

dx.doi.org/10.1021/ja307944d | J. Am. Chem. Soc. 2012, 134, 18591−18598

we can assume that the kinetics of the growth is regulated by the H_2S formation rate and/or its reaction rate with the NPLs surface once complexed with the octylamine ligands. After the addition of TAA and octylamine, the absorption spectrum of the NPLs solution (Figure 3a, middle spectrum) is similar to

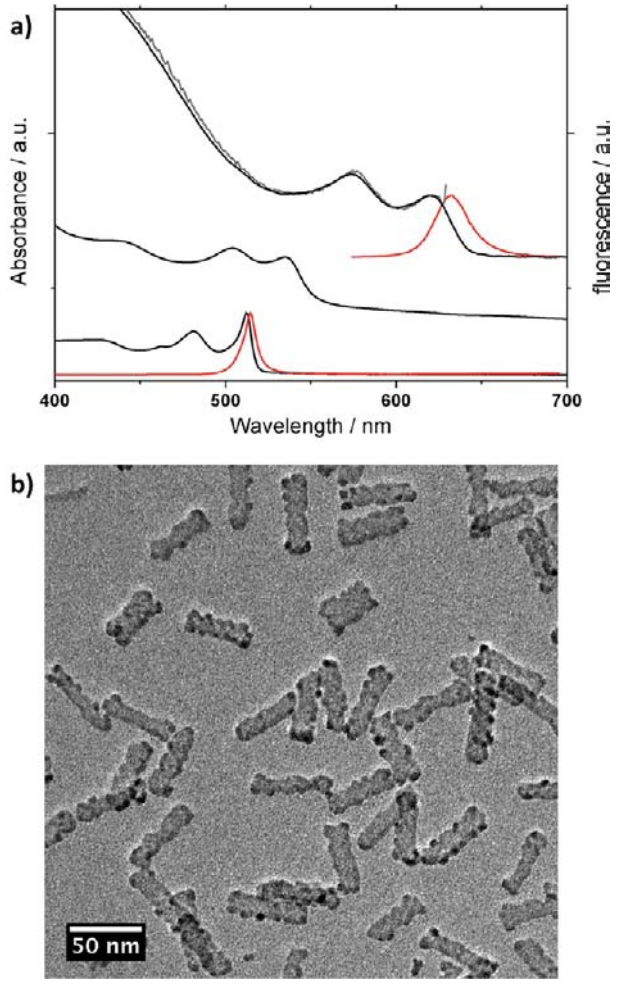

Figure 3. (a) In black, absorbance spectra of the original CdSe nanoplatelets (bottom), after reaction with TAA only (middle), and after continuous CdS shell growth with TAA (top). Fluorescence (red) and photoluminescence excitation (PLE, gray) spectra of CdSe/CdS core/shell nanoplatelets are also reported (top). (b) TEM picture of the corresponding CdSe/CdS core/shell nanoplatelets.

the one obtained for the NPLs after reaction with TMS_2S (Figure 2b). Three hours after the cadmium precursor was added, the core/shell nanoplatelets were purified and isolated from the secondary nucleation of CdS nanocrystals by precipitation with a few drops of ethanol. The resulting NPLs absorption spectrum has substantially shifted to the red with a first excitonic peak around 621 nm and an emission maximum close to 632 nm. These changes of the absorption and fluorescence spectra indicate the shell grown thicker than the one CdS monolayer obtained above (see Figure 2c, top). The thicker CdS shell is also demonstrated by the strong absorption increase below 510 nm (Figure 3a), a value close to the CdS bandgap. The good superposition of the NPL absorption and PL excitation spectra in Figure 3a (top) shows that the aborption increase below 500 nm is only due to CdS shell growth and not to secondary CdS nucleation, which has been removed by the washing step. The TEM images of the NPLs after shell growth (Figure 3b) reveal that the CdS shell is not homogeneous. Some NPLs possess distorted shapes and others have edges with higher contrast than their center, suggesting thickness inhomogeneities. However, even if the shell deposition is not homogeneous, we have demonstrated that we could grow a CdS shell on CdSe NPLs using a continuous reaction process.

CdSe/CdZnS NPLs. On spherical CdSe cores, the shells commonly used to obtain high quantum yield and high photostability are composed of cadmium and zinc sulfides.[7,42−44] We have attempted to reproduce these results on CdSe nanoplatelets, with the growth of CdZnS shells. The lattice mismatch between CdSe and ZnS is close to 13%, and the presence of zinc in the shell should result in even more inhomogeneous NPL shapes. We have thus limited the portion of zinc vs cadmium at 30% into the shell. The growth of a CdZnS shell is performed with a protocol similar to the one used for the CdS shell but with the addition of zinc nitrate as the zinc precursor. Even in the presence of the zinc cation, the shell grows on the NPLs at room temperature. The reaction is monitored by absorption and fluorescence spectroscopy (Figure 4a), and the final core/shell structure presents a first exciton peak at 639 nm and a maximum of emission at 644 nm. The presence of zinc in the shell is confirmed using EDX, in a quantity that is roughly proportional to the amount of zinc nitrate introduced for the shell growth (see Table S1 in Supporting Information). Depending on the surface ligands used after synthesis, CdSe/CdZnS NPLs with quantum yield (QY) as high as 60% have been synthesized (with zinc nitrate and oleic acid treatment, see Experimental Section), and we expect that even higher QY can be obtained with optimized shell composition and surface control.

Surprisingly, on TEM images, the NPLs with CdZnS shell have much more regular shapes than in the case of a pure CdS shell. However, the NPLs CdSe/CdZnS surface is still not perfectly uniform as it appears on the high angle annular dark field (HAADF) images (Figure 4b,c,d). The core/shell structure of the NPLs is clearly visible on the HAADF image (Figure 4d) where a NPL stands on its edge. The difference of atomic density between the core and the shell results in a contrast difference; consequently, the CdSe core clearly stands out against the CdZnS shell. Particularly, in the core, the selenium columns are clearly visible, while in the shell, the sulfur columns are indistinguishable from the background (Figures 4d and S7 in Supporting Information). This HAADF image reveals for the first time the exact number of atomic planes forming the CdSe nanoplatelets. We define a CdSe monolayer as the space between two cadmium planes in the NPL thickness. We can see that the NPL CdSe core emitting initially at 512 mn, contains exactly 4 CdSe monolayers and 5 cadmium planes. Similarly, the CdSe NPL core emitting initially at 553 mn contains exactly 5 CdSe monolayers and 6 cadmium planes (see Figure S7 in Supporting Information). The numbers of monolayers observed in Figure 4d and Figure S7 (in Supporting Information) are two monolayers thinner than the number of monolayers that we estimated previously using a mass effective approach including the nonparabolicity of the conduction and valence bands.[34] The discrepancy we observe could result from the approximation we have performed in our preliminary model where we did neglect the effect of mirror charges,[45] as well as the effect of the dielectric constant used for the calculations.[46] A more precise

dx.doi.org/10.1021/ja307944d | J. Am. Chem. Soc. 2012, 134, 18591−18598

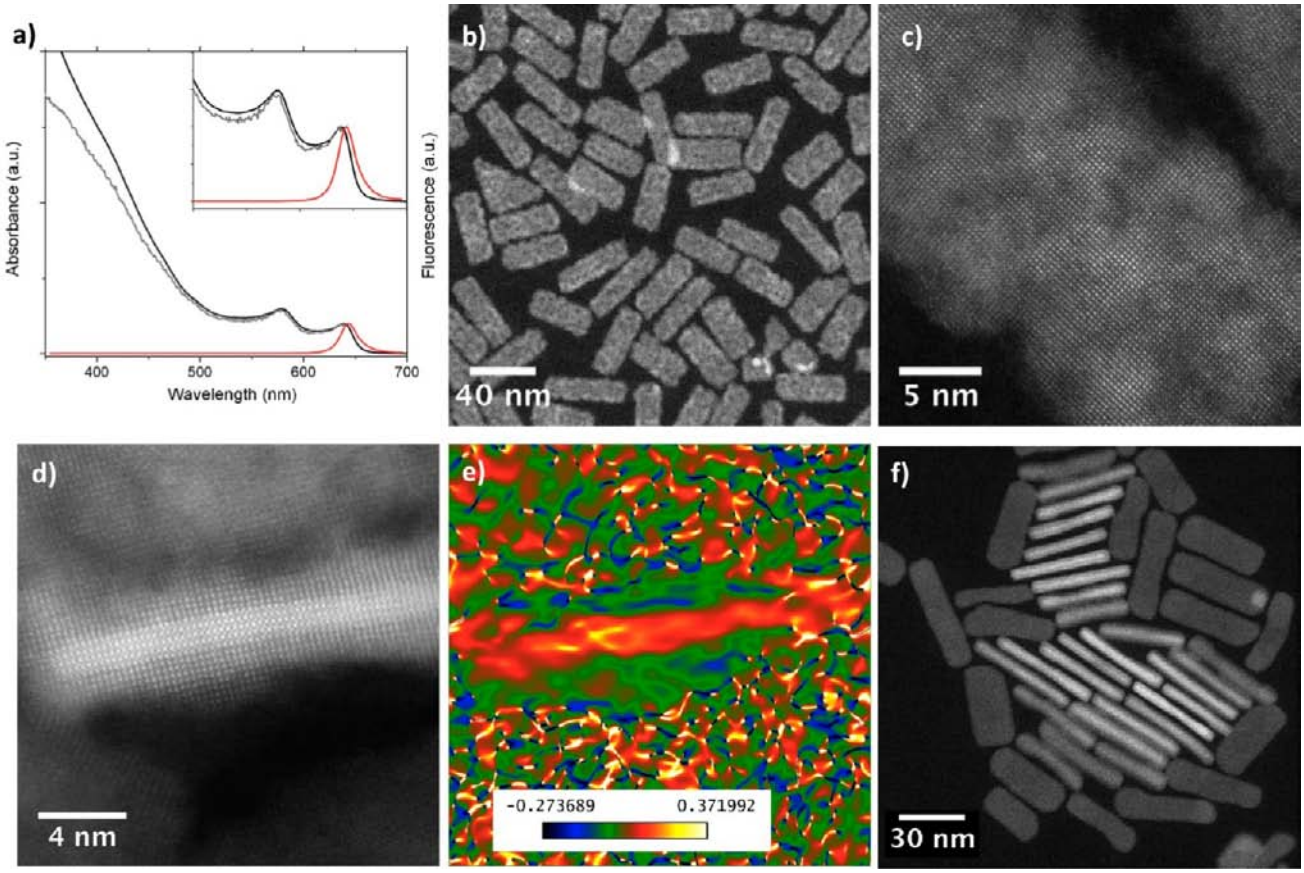

Figure 4. (a) Absorbance (black), fluorescence (red), and photoluminescence excitation (PLE, gray) spectra of the CdSe/$Cd_{0.7}Zn_{0.3}S$ core/shell nanoplatelets obtained with continuous shell growth using TAA. (b) High angle annular dark field (HAADF) image of the resulting core/shell nanoplatelets. (c) High-resolution HAADF picture showing the crystallinity of one nanoplatelet. (d) High-resolution HAADF picture of a core/shell nanoplatelet on the side resolving the core/shell structure and showing the five Cd planes of the initial CdSe nanoplatelet. (e) Geometrical phase analysis (GPA) of the nanoplatelet shown in (d) highlighting the stress between the core and the shell. (f) HAADF picture of an annealed core/shell nanoplatelet sample with very smooth surfaces.

model including the effects of mirror charges should help resolve the discrepancy between the model and the thickness we observe in Figure 4d.[47]

We have analyzed the constraints on the core/shell nanoplatelets using a geometrical phase analysis (GPA) approach. We define the *x*-axis as the direction perpendicular to the NPL plane and the *y*-axis parallel to the largest lateral dimension. Laterally, no contrast is visible on the GPA image (E_{yy} deformation map, Figure S9C in Supporting Information), suggesting that the lattice distances between the core and the shell are equal along the *y*-axis. We assume that, at the surface, the shell material is unconstrained. The core is thus compressed along the lateral dimensions. As the CdSe core is very thin, the strain induced by the shell onto the NPL plane should produce a dilatation of the core along the *x*-axis. The E_{xx} deformation map obtained by GPA (Figures 4e and S9B in Supporting Information) highlights the lattice mismatch between the CdSe core and the CdZnS shell. The deformation measured between the core and the shell reaches up to 14% (Figure S9E in Supporting Information), well above the 8% lattice mismatch between CdSe and $Cd_{0.7}Zn_{0.3}S$, confirming the dilatation. This dilatation of the CdSe core is also confirmed by the direct measurement of the NPLs thicknesses on the HAADF images. NPLs with 4 CdSe monolayers (and 5 Cd planes) in their thickness are 1.4 nm thick instead of the expected 1.2 nm for an unconstrained crystal (4 × 0.3 nm, where 0.3 is half the lattice parameter of CdSe). In the case of NPLs with 5 CdSe monolayers (and 6 Cd planes), NPL are 1.7 nm thick (Figure S7 in Supporting Information) instead of 1.5 nm.

After the shell synthesis, the surface of the core/shell NPLs present irregularities. However, a smooth and homogeneous shell can be obtained using an annealing process. The CdSe/CdZnS NPLs are heated at 300 °C for 30 min in trioctylamine in presence of an excess of cadmium oleate (see Experimental Section). After such treatment, HAADF images (Figures 4f and S8 in Supporting Information) show that the NPLs outer surface does not show any rugosity, and when they lay flat, the contrast observed is much more homogeneous than before annealing (Figure 4b,c). The CdSe core is still clearly visible in the HAADF images (Figure 4f NPLs on their edge, and Figure S8 in Supporting Information), which demonstrates that under these conditions the Zn cations do not diffuse much in the CdSe core. We have therefore shown the possibility to grow a homogeneous 2-nm-thick $Cd_{0.7}Zn_{0.3}S$ shell on CdSe core NPLs. The high strain induced by the shell can be efficiently relaxed by the core because it is very thin.

Even if the shell growth is effective on the different systems tested, there is a huge homogeneity difference between the CdS and the $Cd_{0.7}Zn_{0.3}S$ shell deposition as evidenced by the TEM pictures. Lattice mismatch between the core and the shell is a common source of defects and inhomogeneities during the shell growth. The effect of lattice mismatch between two

dx.doi.org/10.1021/ja307944d | *J. Am. Chem. Soc.* 2012, 134, 18591−18598

epitaxially grown films has been extensively documented[48] and can lead to the formation of islands as in the Stranski-Krastanov process. In our case, because the lattice mismatch between CdSe and CdS (4%) is lower than in the CdSe and $Cd_{0.7}Zn_{0.3}S$ (8%), we expected more regular CdSe/CdS NPLs than CdSe/$Cd_{0.7}Zn_{0.3}S$ NPLs. But, as demonstrated above, the shell growth on NPLs is epitaxial thanks to the relaxation of the strains by core deformation. The heterogeneity during the shell growth could also be due to polytypism in the shell material. As previously described for CdSe/CdS quantum dots, when a CdS shell is grown on a zinc blende spherical CdSe core in the presence of primary amines, the shell grows with a wurtzite or a polytypic structure.[22] The growth of a wurtzite shell on a zinc blende (zb) core generally promotes a preferential growth perpendicular to the zb[111] planes,[49] localized on the NPL corners. Indeed, the CdSe/CdS core/shell NPLs present CdS outgrowths on their corners (Figure 3b), but the supposed polytypism of the CdS shell does not appear on the powder X-ray diffractogram realized on this sample (see Figure S10 in Supporting Information). This is maybe due to the limited quantity of the shell material, because when a thicker CdS shell is grown, the outgrowths are more developed (Figure S11 in Supporting Information) and polytypism is observed in the X-ray diffractogram. On the contrary, the CdSe/$Cd_{0.7}Zn_{0.3}S$ core/shell NPLs exhibit pure zinc blende crystalline structure. This possible polytypism in the shell crystal structure observed for the CdSe/CdS but not for the CdSe/$Cd_{0.7}Zn_{0.3}S$ core/shell NPLs provides a first insight to explain the differences in shapes. An alternative explanation for the shape difference is illustrated Figure S12 (in Supporting Information) and relies on the outgrowth density of the shell on the core CdSe nanoplatelets. We observe in Figure S12 (in Supporting Information) that, for CdS shells, the number of outgrowths per nanoplatelet visible on the edges is small (about ten). When 10% of zinc is added to the reaction mixture, the outgrowth number increases up to being almost indistinguishable. At 30% of zinc in the shell, the CdZnS overlayer appears nearly homogeneous. This behavior may come from a difference of heterogeneous nucleation density or from an Ostwald ripening process dependent on the zinc concentration.

We have demonstrated the growth of shells on CdSe NPLs originally emitting at 512 or 553 nm with small lateral dimensions (<40 nm). To show the robustness of the shell growth, we tested thin CdS growth on large CdSe nanosheets. We can synthesize thinner (first exciton around 462 nm) NPLs with lateral dimensions that can reach a few hundred nanometers. These NPLs fold on themselves in solution to form nanoscrolls (Figure 5b); the reason for this folding in solution is not clear but is probably related to the asymmetric elastic constraint that the carboxylate ligand exerts upon the two large facets of the CdSe nanosheet. We use the same protocol as that developed for the continuous growth of CdS shell on CdSe nanoplatelets. In spite of the initial folding of the CdSe nanosheets, a CdS shell grows, and we obtain CdSe/CdS nanosheets with an absorption spectrum similar to the one obtained for the smaller NPLs (Figure 5a). As the shell grows, the nanosheets unfold, and we obtain flat nanosheets with lateral dimensions that can reach 300 nm (Figure 5c). The unfolding of the nanoscrolls can result from the removal of the carboxylic acid ligand, or from the increase in the thickness of the nanosheet that makes it more rigid, or from both. The possibility to grow in solution core/shell 2D structures with lateral dimensions of several hundred nanometers adds up to the already fantastic tool box made of colloidal nanoparticles with different sizes and shapes.

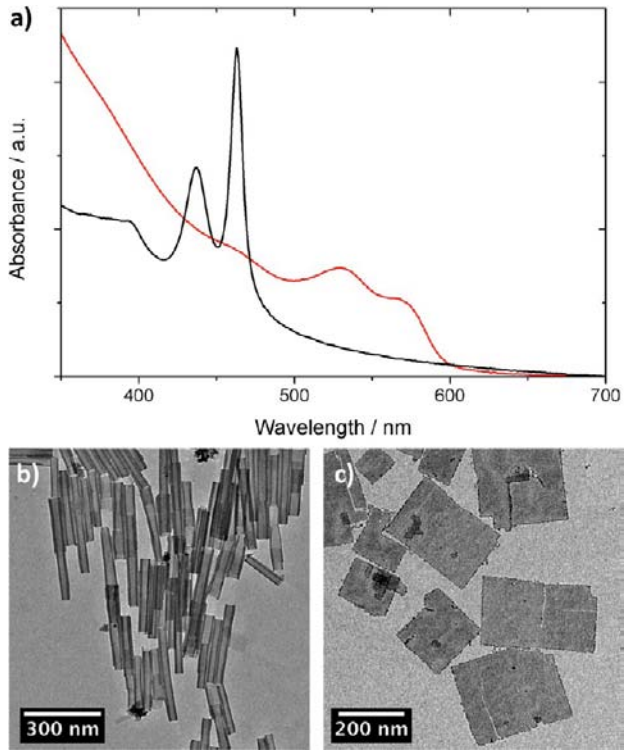

Figure 5. Absorbance spectrum of extended CdSe nanoplatelets before/after CdS shell growth. (b) TEM picture of the extended nanoplatelets. (c) TEM of the same NPLs after CdS growth.

CONCLUSION

We have demonstrated the growth of a shell on CdSe 2D structures. The protocol for shell growth was tested on core nanoplatelets with different thicknesses (3, 4, and 5 CdSe monolayers) and lateral dimensions (from 20 nm up to 300 nm). To the best of our knowledge, we have reported here one of the first room-temperature syntheses in organic solvent of a semiconductor shell on a colloidal semiconductor core. We have shown that this shell could be grown using a layer-by-layer process but more interestingly using a continuous shell growth in a one-pot approach.

The thioacetamide-based shell growth we developed has the following characteristics. First, even if there is some secondary nucleation, the growth does not occur preferentially on these nuclei but on the cores present in solution, and this secondary nucleation is easily separated from the NPLs because of their size difference. Second, as the reaction rate is driven by the slow reaction between the TAA and the octylamine, it can be simply controlled with the temperature and the concentration of octylamine. Third, continuous and slow injection protocols for shell growth can be avoided by the slow release of the active species (probably H_2S) in solution, and a "one-pot" shell growth protocol can be implemented. A more detailed study of the shell growth using thioacetamide as sulfide precursor is currently under investigation.

The effective formation of shells has been verified by absorption spectroscopy and by direct imaging using a STEM-HAADF setup. We have obtained unambiguous evidence of the core/shell structure, the difference of atomic density between the core and the shell resulting in contrast difference on the

dx.doi.org/10.1021/ja307944d | J. Am. Chem. Soc. 2012, 134, 18591−18598

STEM-HAADF pictures. Moreover, a careful analysis of the deformations inside the nanoplatelet using geometrical phase analysis (GPA) reveals a tetragonal deformation of the CdSe core. The ability of the thin initial CdSe nanoplatelet to bear such deformations allows epitaxial growth of the CdZnS shell.

These colloidal core/shell structures are remarkable in the sense that they are the first step toward the synthesis of colloidal multiple quantum wells similar to the ones grown by MBE and MOCVD and that have already found several applications in the field of optoelectronic. As for the core/shell NCs, core/shell nanoplatelets should have more robust optical properties and may introduce an interesting field of research.

EXPERIMENTAL SECTION

All materials were purchased from Sigma-Aldrich and used without any further purification.

CdSe Nanoplatelet Synthesis. 90 mL of 1-octadecene, 480 mg of cadmium acetate dihydrate ($Cd(OAc)_2(H_2O)_2$), and 1.18 g of oleic acid were introduced into a 250 mL three-neck flask. The mixture was degassed under vacuum and magnetic stirring at 110 °C during 90 min. After inerting the flask with argon, 72 mg of elemental Se powder dispersed in 2 mL ODE was swiftly injected in the hot mixture and the temperature was set to 240 °C. When the temperature reached 205 °C, 240 mg of $Cd(OAc)_2(H_2O)_2$ was introduced in the reaction mixture and the reaction was allowed to proceed 15 min at 240 °C. The mixture was then cooled down to room temperature and 10 mL oleic acid was added, inducing the aggregation of the platelets. The mixture was centrifuged 10 min at 5000 rpm, the supernatant was discarded, and the precipitated nanoplatelets were suspended in hexane. The platelets were then precipitated one more time with ethanol and suspended in 10 mL hexane.

Ligand Exchange with Dodecanethiol. 400 μL of the as-synthetized nanoplatelets in hexane was diluted in 2 mL hexane and 200 μL dodecanethiol. The mixture was heated at 65 °C during 24 h to allow a complete ligand exchange.

Layer by Layer CdS Shell Growth using TMS_2S and $Cd(oleate)_2$. 400 μL of the as-synthetized nanoplatelets in hexane was diluted in 2 mL hexane. In a glovebox, 100 μL of Bis(trimethylsilyl) sulfide (TMS_2S) was introduced into the yellow solution of platelets and allowed to react for 1 h. The color of the solution quickly shifted from yellow to orange, and the platelets began to aggregate with each other, troubling the solution. The resulting nanocrystals were washed 2 times with ethanol and dispersed in hexane. Because of the lack of ligands, the nanocrystals were aggregated. Thirty milligrams of $Cd(OAc)_2(H2O)_2$ was then added and the mixture was sonicated for 10 min, inducing another color change from orange to red. Adding 200 μL of oleic acid induced the disaggregation of the core/shell platelets and the formation of a clear red-colored solution.

Continuous CdS Shell Growth Using Thioacetamide and $Cd(oleate)_2$. 400 μL of the as-synthetized nanoplatelets in hexane was diluted in 2 mL chloroform. Twenty milligrams of thioacetamide (TAA) and 200 μL of octylamine were added in the flask and the mixture was sonicated until the complete dissolution of the TAA (about 5 min). The color of the solution changed from yellow to orange in about 10 min. 200 μL of a 0.1 M $Cd(oleate)_2$ solution in octylamine was then added to the reaction mixture. The reaction was allowed to proceed for 3 h at room temperature. An important secondary nucleation occurred but the growth of the CdS shell on the initial CdSe platelets was still effective. After synthesis, the core/shell platelets were isolated from the secondary nucleation by precipitation with a few drops of ethanol and suspended in $CHCl_3$. To improve the quantum yield and the dispersion, the final core/shell platelets were capped with $Cd(oleate)_2$ and isolated with UV light for one hour.

Continuous $Cd_{0.7}Zn_{0.3}S$ Shell Growth Using Thioacetamide. One milliliter of the as-synthetized nanoplatelets in hexane was diluted in 4 mL chloroform. 100 mg of thioacetamide (TAA) and 1 mL of octylamine were added in the flask and the mixture was sonicated until complete dissolution of the TAA (about 5 min). The color of the solution changed from yellow to orange during this time. 350 μL of a solution of $Cd(NO_3)_2$ 0.2 M in ethanol and 150 μL of a solution of $Zn(NO_3)_2$ 0.2 M in ethanol are then added to the flask. The reaction was allowed to proceed for 24 h at room temperature. After synthesis, the core/shell platelets were isolated from the secondary nucleation by precipitation with a few drops of ethanol and suspended in 5 mL $CHCl_3$. To improve the stabilization and the quantum yield of the core/shell nanoplatelets, 100 μL of $Zn(NO_3)_2$ 0.2 M in ethanol is added to the NPLs solution. They aggregate steadily and are resuspended by adding 200 μL oleic acid. At this time, their quantum yield is low and is recovered over a few days.

Core/Shell Nanoplatelets Annealing. Ten milliliters of trioctylamine (TOA), 2.5 mL of the CdSe/CdZnS core/shell nanoplatelets as prepared above, and 1 mL of $Cd(oleate)_2$ 0.5 M in oleic acid are introduced in a three-neck flask. After 30 min of degassing under vacuum at 70 °C, the solution under argon is heated up to 300 °C and maintained at this temperature for 30 min. The solution is then cooled at room temperature and the platelets are precipitated with ethanol and suspended in hexane.

Application of the CdS Continuous Growth to Unfold Large Nanosheets. The CdS shell growth protocol described above is applied on large CdSe nanoplatelets with minor modification. The reaction was allowed to proceed for 30 min instead of 3 h at room temperature. The large CdSe nanoplatelets synthesis is described in Supporting Information.

ASSOCIATED CONTENT

Supporting Information

Additional experimental details and figures, Table of EDX quantitative analysis and X-ray powder diffractograms. This material is available free of charge via the Internet at http://pubs.acs.org.

AUTHOR INFORMATION

Corresponding Author

benoit.dubertret@espci.fr

Notes

The authors declare no competing financial interest.

ACKNOWLEDGMENTS

B.D. thanks P. Voisin for fruitful discussions and X. Xu for help with the TEM maintenance.

REFERENCES

(1) Ekimov, A. I.; Onushchenko, A. A. *Jetp Lett.* **1981**, *34*, 345.
(2) Murray, C. B.; Norris, D. J.; Bawendi, M. G. *J. Am. Chem. Soc.* **1993**, *115*, 8706.
(3) Peng, X. G.; Manna, L.; Yang, W. D.; Wickham, J.; Scher, E.; Kadavanich, A.; Alivisatos, A. P. *Nature* **2000**, *404*, 59.
(4) Yu, H.; Li, J. B.; Loomis, R. A.; Gibbons, P. C.; Wang, L. W.; Buhro, W. E. *J. Am. Chem. Soc.* **2003**, *125*, 16168.
(5) Ithurria, S.; Dubertret, B. *J. Am. Chem. Soc.* **2008**, *130*, 16504.
(6) Hines, M. A.; GuyotSionnest, P. *J. Phys. Chem.* **1996**, *100*, 468.
(7) Talapin, D. V.; Mekis, I.; Gotzinger, S.; Kornowski, A.; Benson, O.; Weller, H. *J. Phys. Chem. B* **2004**, *108*, 18826.
(8) Chen, Y.; Vela, J.; Htoon, H.; Casson, J. L.; Werder, D. J.; Bussian, D. A.; Klimov, V. I.; Hollingsworth, J. A. *J. Am. Chem. Soc.* **2008**, *130*, 5026.
(9) Mahler, B.; Spinicelli, P.; Buil, S.; Quelin, X.; Hermier, J. P.; Dubertret, B. *Nat. Mater.* **2008**, *7*, 659.
(10) Michalet, X.; Pinaud, F. F.; Bentolila, L. A.; Tsay, J. M.; Doose, S.; Li, J. J.; Sundaresan, G.; Wu, A. M.; Gambhir, S. S.; Weiss, S. *Science* **2005**, *307*, 538.
(11) Qian, L.; Zheng, Y.; Xue, J. G.; Holloway, P. H. *Nat. Photonics* **2011**, *5*, 543.

(12) Lee, J. S.; Kovalenko, M. V.; Huang, J.; Chung, D. S.; Talapin, D. V. *Nat. Nanotechnol.* **2011**, *6*, 348.
(13) Ithurria, S.; Guyot-Sionnest, P.; Mahler, B.; Dubertret, B. *Phys. Rev. Lett.* **2007**, *99*, 4.
(14) Smith, A. M.; Mohs, A. M.; Nie, S. *Nat. Nanotechnol.* **2009**, *4*, 56.
(15) Yu, Z. H.; Guo, L.; Du, H.; Krauss, T.; Silcox, J. *Nano Lett.* **2005**, *5*, 565.
(16) Son, D. H.; Hughes, S. M.; Yin, Y. D.; Alivisatos, A. P. *Science* **2004**, *306*, 1009.
(17) Park, J.; Zheng, H.; Jun, Y. W.; Alivisatos, A. P. *J. Am. Chem. Soc.* **2009**, *131*, 13943.
(18) Cragg, G. E.; Efros, A. L. *Nano Lett.* **2010**, *10*, 313.
(19) Wang, X.; Ren, X.; Kahen, K.; Hahn, M. A.; Rajeswaran, M.; Maccagnano-Zacher, S.; Silcox, J.; Cragg, G. E.; Efros, A. L.; Krauss, T. D. *Nature* **2009**, *459*, 686.
(20) Carbone, L.; Nobile, C.; De Giorg, M.; Sala, F. D.; Morello, G.; Pompa, P.; Hytch, M.; Snoeck, E.; Fiore, A.; Franchini, I. R.; Nadasan, M.; Silvestre, A. F.; Chiodo, L.; Kudera, S.; Cingolani, R.; Krahne, R.; Manna, L. *Nano Lett.* **2007**, *7*, 2942.
(21) Talapin, D. V.; Koeppe, R.; Gotzinger, S.; Kornowski, A.; Lupton, J. M.; Rogach, A. L.; Benson, O.; Feldmann, J.; Weller, H. *Nano Lett.* **2003**, *3*, 1677.
(22) Mahler, B.; Lequeux, N.; Dubertret, B. *J. Am. Chem. Soc.* **2010**, *132*, 953.
(23) Chen, O.; Yang, Y. A.; Wang, T.; Wu, H. M.; Niu, C. G.; Yang, J. H.; Cao, Y. C. *J. Am. Chem. Soc.* **2011**, *133*, 17504.
(24) Lim, S.-J.; Kim, W.; S.K., S. *J. Am. Chem. Soc.* **2012**, *134*, 7576.
(25) Donega, C. D. *Chem. Soc. Rev.* **2011**, *40*, 1512.
(26) Reiss, P.; Protiere, M.; Li, L. *Small* **2009**, *5*, 154.
(27) Manna, L.; Scher, E. C.; Li, L. S.; Alivisatos, A. P. *J. Am. Chem. Soc.* **2002**, *124*, 7136.
(28) Cassette, E.; Mahler, B.; Guigner, J.-M.; Patriarche, G.; Dubertret, B.; Pons, T. *ACS Nano* **2012**, *6*, 6741.
(29) Narukawa, Y.; Kawakami, Y.; Fujita, S.; Fujita, S.; Nakamura, S. *Phys. Rev. B* **1997**, *55*, R1938.
(30) Joo, J.; Son, J. S.; Kwon, S. G.; Yu, J. H.; Hyeon, T. *J. Am. Chem. Soc.* **2006**, *128*, 5632.
(31) Liu, Y. H.; Wayman, V. L.; Gibbons, P. C.; Loomis, R. A.; Buhro, W. E. *Nano Lett.* **2010**, *10*, 352.
(32) Ithurria, S.; Bousquet, G.; Dubertret, B. *J. Am. Chem. Soc.* **2011**, *133*, 3070.
(33) Fritzinger, B.; Capek, R. K.; Lambert, K.; Martins, J. C.; Hens, Z. *J. Am. Chem. Soc.* **2010**, *132*, 10195.
(34) Ithurria, S.; Tessier, M. D.; Mahler, B.; Lobo, R. P. S. M.; Dubertret, B.; Efros, A. L. *Nat. Mater.* **2011**, *10*, 936.
(35) Knowles, K. E.; Frederick, M. T.; Tice, D. B.; Morris-Cohen, A. J.; Weiss, E. A. *J. Phys. Chem. Lett.* **2012**, *3*, 18.
(36) Bullen, C.; Mulvaney, P. *Langmuir* **2006**, *22*, 3007.
(37) Caldwell, M. A.; Albers, A. E.; Levy, S. C.; Pick, T. E.; Cohen, B. E.; Helms, B. A.; Milliron, D. J. *Chem. Commun.* **2011**, *47*, 556.
(38) Owen, J. S.; Park, J.; Trudeau, P. E.; Alivisatos, A. P. *J. Am. Chem. Soc.* **2008**, *130*, 12279.
(39) Tschirner, N.; Lange, H.; Schliwa, A.; Biermann, A.; Thomsen, C.; Lambert, K.; Gomes, R.; Hens, Z. *Chem. Mater.* **2012**, *24*, 311.
(40) Blackman, B.; Battaglia, D.; Peng, X. G. *Chem. Mater.* **2008**, *20*, 4847.
(41) Thomson, J. W. T. J. W.; Nagashima, K.; Macdonald, P. M.; Ozin, G. A. *J. Am. Chem. Soc.* **2011**, *133*, 5036.
(42) Xie, R.; Kolb, U.; Li, J.; Basché, T.; Mews, A. *J. Am. Chem. Soc.* **2005**, *127*, 7480.
(43) Jun, S.; Jang, E.; Lim, J. E. *Nanotechnology* **2006**, *17*, 3892.
(44) Steckel, J. S.; Snee, P.; Coe-Sullivan, S.; Zimmer, J. R.; Halpert, J. E.; Anikeeva, P.; Kim, L. A.; Bulovic, V.; Bawendi, M. G. *Angew. Chem., Int. Ed.* **2006**, *45*, 5796.
(45) Mosko, M.; Munzar, D.; Vagner, P. *Phys. Rev. B* **1997**, *55*, 15416.
(46) Senger, R. T.; Bajaj, K. K. *Phys. Rev. B* **2003**, *68*, 205314.
(47) Benchamekh, R.; Even, J.; Jancu, J. M.; Nestoklon, M.; Ithurria, S.; Dubertret, B.; Voisin, P. In *20th International Symposium "Nanostructures: Physics and Technology"*; St. Petersburg Academic University; Nizhny Novgorod, Russia, 2012.
(48) Vandermerwe, J. H. *J. Appl. Phys.* **1963**, *34*, 123.
(49) Milliron, D. J.; Hughes, S. M.; Cui, Y.; Manna, L.; Li, J. B.; Wang, L. W.; Alivisatos, A. P. *Nature* **2004**, *430*, 190.